ICOS-Ligand Triggering Impairs Osteoclast Differentiation and Function In Vitro and In Vivo

ICOS-Ligand triggering impairs osteoclast differentiation and function in vitro and in vivo..
Casimiro L. Gigliotti,1, Elena Boggio*,1, Nausicaa Clemente*, Yogesh Shivakumar*, Erika Toth*, Daniele Sblattero*, Patrizia D'Amelio†, Giancarlo Isaia†, Chiara Dianzani‡, Junji Yagi§, Josè M. Rojo¶, Annalisa Chiocchetti*, Renzo Boldorini*, Michela Bosetti||, and Umberto Dianzani*..*
J Immunol. 2016 Nov 15;197(10):3905-3916.

ICOS-Ligand triggering impairs osteoclast differentiation and function *in vitro* and *in vivo*.

Running title: ICOSL function in osteoclasts

Casimiro L. Gigliotti[*,1], Elena Boggio[*,1], Nausicaa Clemente[*], Yogesh Shivakumar[*], Erika Toth[*], Daniele Sblattero[*], Patrizia D'Amelio[†], Giancarlo Isaia[†], Chiara Dianzani[‡], Junji Yagi[§], Josè M. Rojo[¶], Annalisa Chiocchetti[*], Renzo Boldorini[*], Michela Bosetti[‖], and Umberto Dianzani[*].

[*]Interdisciplinary Research Center of Autoimmune Diseases (IRCAD) and Department of Health Sciences, University of Piemonte Orientale (UPO), 28100 Novara, Italy; [†]Department of Medical Sciences, University of Torino, 10125 Torino, Italy; [‡]Department of Drug Science and Technology, University of Torino, 10125 Torino, Italy; [§]Department of Microbiology and Immunology, Tokyo Women's Medical University, Tokyo 108-8639, Japan; [¶]Departamento de Medicina Celular y Molecular, Centro de Investigaciones Biologicas, Consejo Superior de Investigaciones Cientıficas, 28006 Madrid, Spain; [‖]Department of Pharmaceutical Sciences, UPO, 28100 Novara, Italy.

[1] C. L. G. and E. B. contributed equally to this work.

Corresponding Author:

Umberto Dianzani, UPO, Via Solaroli 17 28100, Novara, Italy; Tel:+39-0321-660644, Fax:+39-0321-620421; e-mail: umberto.dianzani@med.uniupo.it

Grant Support

This research was supported by the Associazione Italiana Ricerca sul Cancro (IG 14430, AIRC, Milan), Fondazione Amici di Jean (Torino), and Fondazione Cassa di Risparmio di Cuneo (Cuneo).

Abbreviations used

DC, dendritic cells; EC, endothelial cells; OCs, osteoclasts; RANK, receptor activator of nuclear factor-kappa B; RANKL, RANK ligand; MMPs, metalloproteinases; OPG, Osteoprotegerin; TRAP, tartrate resistant acid phosphatase; RA, rheumatoid arthritis; OBs, osteoblasts; MDOCs, monocytes-derived OCs; Th, T helper; Treg, regulatory T cells.

ABSTRACT

Osteoblasts, osteocytes, and osteoclasts (OCs) are involved in the bone production and resorption which are crucial in bone homeostasis. OCs hyperactivation plays a role in the exaggerated bone resorption of diseases such as osteoporosis, rheumatoid arthritis, and osteolytic tumor metastases. This work stems from the finding that OCs can express B7h (or ICOS-Ligand) which is the ligand of the ICOS T cell costimulatory molecule. Since recent reports have shown that, in endothelial cells, dendritic cells and tumor cells, B7h triggering modulates several activities of these cells, we analysed the effect of B7h triggering by recombinant ICOS-Fc on OCs differentiation and function. The results showed that ICOS-Fc inhibits RANKL-mediated differentiation of human monocytes to OCs by inhibiting the acquirement of the OCs morphology, the $CD14^-$ Cathepsin K^+ phenotype, and the expression of tartrate resistant acid phosphatase, OSCAR, NFATc1, and DC-STAMP. Moreover, ICOS-Fc induces a reversible decrease in the sizes of cells and number of nuclei and Cathepsin K expression in mature OCs. Finally, ICOS-Fc inhibits the osteolytic activities of OCs *in vitro*, and the development of bone loss in ovariectomized or soluble RANKL treated mice. These data open a novel field in the pharmacological use of agonists and antagonists of the ICOS/B7h system.

Introduction

B7h (CD275, also known as ICOSL, B7H2, B7-RP1, GL50) belongs to the B7 family of surface receptors and it binds ICOS (CD278), which belongs to the CD28 family (1-5). ICOS is expressed by activated T cells, whereas B7h is expressed by a wide variety of cell types, including B cells, macrophages, and dendritic cells (DC). However, B7h is also expressed by cells of non haemopoietic origin such as vascular endothelial cells (EC), epithelial cells, and fibroblasts, and many tumor cells. The main known function of B7h is the triggering of ICOS, which acts as a costimulatory molecule for activated T cells by modulating their cytokine secretion and, particularly, increasing the secretion of IFN-γ (in humans), IL-4 (in mice), IL-10, IL-17, and IL-21 (in both species) (6-11). However, recent reports have shown that the B7h:ICOS interaction can trigger bidirectional signals able to modulate also the response of the B7h-expressing cells. In mouse DC, this B7h-mediated "reverse signalling" induces partial maturation with prominent augmentation of IL-6 secretion (12). In human DC, it modulates cytokine secretion, promotes the capacity to cross-present endocytosed antigens in class I MHC molecules, and inhibits adhesiveness to EC and migration (13,14). B7h stimulation also inhibits the adhesiveness and migration of EC and tumor cell lines *in vitro* and development of experimental lung metastases *in vivo* (15,16). These effects are accompanied by decreased phosphorylation of ERK and p38 in EC; decreased phosphorylation of focal adhesion kinase and down-modulation of β-Pix in EC and tumor cells. Moreover, triggering of B7h potentiates signaling via several pattern recognition receptors in human DC through a signaling pathway involving the adaptor protein Receptor for activated C kinase 1 (RACK1) and the kinases protein kinase C (PKC) and JNK (14).

The aim of our research was to extend these analyses by investigating the expression and function of B7h in osteoclasts (OCs) which derive from the monocyte lineage, similarly to DC. OCs are giant cells formed by the cell-cell fusion of monocyte-macrophage precursors and characterized by multiple nuclei, abundant vacuoles, and lysosomes; they play a key role in bone remodelling, which

involves also osteoblasts (OBs) and osteocytes. OCs differentiate from monocytes under the influence of M-CSF and receptor activator of nuclear factor-kappa B ligand (RANKL) (17-21).

The OCs function is stimulated by the triggering of receptor activator of nuclear factor-kappa B RANK expressed on the membrane of OCs by RANKL. In healthy bone, RANKL is mainly expressed by OBs as a surface receptor in response to bone-resorbing factors and it is cleaved into a soluble molecule by metalloproteinases (MMPs). Moreover, RANKL is also expressed by stromal cells, lymphocytes, and macrophages which can support OCs function during inflammation. Osteoprotegerin (OPG) is a soluble decoy receptor of RANKL secreted by OBs and stromal cells; OPG prevents RANK stimulation by inhibiting its binding to RANKL and impairs osteoclastogenesis (22). The binding of M-CSF to its colony-stimulating factor 1 receptor (c-fms) on OCs progenitors upregulates expression of RANK on these cells and is essential for osteoclastogenesis (23). OCs differentiation includes cell polarization with formation of ruffled membrane and sealing of the OCs to the bone to form a sealing zone, or clear zone, that separates the resorption lacunae from the surround. This is the secretion site of acid, tartrate resistant acid phosphatase (TRAP), cathepsins, and MMPs leading to demineralization of the inorganic component of the bone and hydrolysis of its organic components (17,18). During physiological remodelling, after bone resorption, OBs are recruited within the resorption site and the resorption lacuna is filled with bone matrix secreted by these cells; the matrix will then be mineralized by precipitation of hydroxyapatite crystals (21).

Increased OCs activity leads to bone loss and can be detected in conditions such as osteoporosis, rheumatoid arthritis (RA), and other autoimmune diseases, in which a key role has been ascribed to inflammatory cytokines and adaptive immunity (24). Moreover, some neoplasia involving immune cells, such as multiple myeloma, are characterized by intense focal bone erosions ascribed to high expression of RANKL by stromal cells and, possibly, myeloma cells. Furthermore, bone metastases of solid cancer may be osteolytic through expression of a soluble form of RANKL (25,26).

Several inflammatory cytokines, such as TNFα, IL-1, IL-6, and M-CSF upregulate RANKL

116 expression and stimulate OCs function (27-29). A key role is played by type 17 T helper (Th17)
117 cells secreting IL-17, which induces the expression of RANKL in OBs and synovial cells.
118 Moreover, IL-17 supports recruitment of several immune cell types producing cytokines and other
119 proinflammatory molecules supporting OCs differentiation and activity (30).
120 Our research analyzed the effect of B7h triggering by ICOS-Fc on OCs differentiation and function
121 both *in vitro* and *in vivo*. The results showed that OCs express B7h during their differentiation, and
122 that B7h triggering reversibly inhibits OCs differentiation and function both *in vitro* and *in vivo.*
123

Materials and Methods

Cells

PBMC were separated from human blood samples obtained from healthy donors, who signed their written informed consent, by density gradient centrifugation using the Ficoll-Hypaque reagent (Limpholyte-H, Cedarlane Laboratories, Burlington, ON, Canada). Monocytes derived OCs (MDOCs) were prepared from $CD14^+$ monocytes isolated with the EasySep^{TM}Human CD14 Negative Selection Kit (StemCells Techologies, Vancouver, BC,USA). Monocytes ($0.5x10^6$) were plated in a 24-wells plate and cultured for 21 d in a differentiation medium composed of DMEM (Invitrogen, Burlington, ON, Canada), 2 mM L-glutamine, 10% FBS (Invitrogen), recombinant human M-CSF (25 ng/ml; R&D System, Minneapolis, MN, USA) and RANK-L (30 ng/ml; R&D Systems). The differentiation medium was changed every 3 d. At different times (Fig. S1A), cells were treated with 1 μg/ml of either ICOS-Fc (a fusion protein of the extracellular portion of the human ICOS fused to the human IgG1 Fc portion) or ICOS-msFc composed of the human ICOS fused to the mouse IgG1 Fc. Controls were performed using ^{F119S}ICOS-Fc, carrying the F119S substitution in the human ICOS amino acid sequence. For analysis, MDOCs were detached from the plates using the Tryple express reagent (Life Technologies, Carlsbad, CA, USA) for 15 minutes before using a cell scraper (31). Cell viability detected by Trypan blue exclusion assay was >98%.

Immunofluorescence

The OCs phenotype was assessed by immunofluorescence and flow cytometry (BD, Bioscience, San Diego, CA, USA) using the FITC-, PE-, and Allophycocyanin-conjugated monoclonal antibodies to CD14 (Immunotools, Frieosythe, Germany), Catepsin-K (Bioss Inc., Woburn, MA,USA), and B7h (R&D Systems). Catepsin-K was evaluated after cell permeabilization using the FIX and PERM kit (Invitrogen).

Actin and B7h staining were performed on cells cultured on glass coverslips, fixed with 4% paraformaldehyde and then permeabilized with 5% FBS, 1% bovine BSA and 0.1% Triton X-100.

Then, cells were stained with anti B7h rabbit polyclonal antibodies (Bioss Inc.) or preimmune rabbit Ig followed by Texas Red-conjugated secondary anti-rabbit Ig (Invitrogen), or with Tetramethylrhodamine B isothiocyanate (TRITC)-conjugated phalloidin (Sigma-Aldrich, St Louis, MO, USA) in a solution of 0.1% Triton X-100, 1% BSA, 2% FBS. Nuclear chromatin was stained with the fluorescent dye 4,6-diamidino-2-phenylindole-dihydrochloride (DAPI, Sigma-Aldrich). Stained cells were mounted with Slow-FADE (Light AntiFADE Kit, Molecular Probes Invitrogen) and observed by a fluorescence Leica DM 2500 fluorescence microscope equipped with a DFC7000 camera (all from Leica Microsystems, Milan, Italy); data were analyzed with Leica QWin Plus V 2.6 imaging software.

Western blot

MDOCs were lysed in 50 mM Tris-HCl pH 7.4, 150 mM NaCl, 5 mM EDTA, 1% NP-40 with phosphatase and protease inhibitor cocktails (Sigma-Aldrich). Then, 30 μg of proteins were run on 10% SDS PAGE gels and transferred onto Hybond-C extra nitrocellulose membranes (Ge Healthcare, Piscataway, NJ, USA). The membranes were then probed with antibodies to B7h (Bioss Inc.), phospho and total -p38 MAPK, -Erk1,2, -JNK, phospho-PKC (Cell Signaling Technology, Danvers, MA, USA), β-Pix (Millipore, Billerica, MA,USA), and β-actin (Sigma-Aldrich), followed by HRP-conjugated secondary antibodies (Sigma-Aldrich). The bands were detected via chemiluminescence using the VersaDoc Imaging System (Bio-Rad Laboratories, Hercules, CA, USA).

Proliferation assay

Monocytes ($1x10^3$/well) were seeded in 96-well plates and incubated at 37°C, 5% CO_2, for 3 d. Cells were treated with ICOS-Fc (1 μg/ml) in complete medium with or without M-CSF (25 ng/ml). After 3 d of incubation, viable cells were evaluated by 2,3-bis[2-methoxy-4-nitro-5sulphophenyl]-

2H-tetrazolium-5carboxanilide (MTT, Sigma-Aldrich) inner salt reagent at 570 nm, as described by the manufacturer's protocol. The controls (i.e. cells that had received no treatments) were normalized to 100%, and the readings from treated cells were expressed as % of controls.

Real-Time RT-PCR

Total RNA was isolated from MDOCs cultures at d 7 (T7), d 14 (T14), and d 21 (T21) or from mice bone tissue (total limbs including scapula and pelvis), using TRIzol reagent (Invitrogen). RNA (500 ng) was retrotranscribed using the QuantiTect Reverse Transcription Kit (Qiagen, Hilden, Germany). DC-STAMP, OSCAR, NFATc1, and B7h expression were evaluated with a gene expression assay (Assay-on Demand, Applied Biosystems, Foster City, CA, USA). The glyceraldehyde 3-phosphate dehydrogenase (GAPDH) gene was used to normalize the cDNA amounts. Real Time PCR was performed using the CFX96 System (Bio-Rad Laboratories) in duplicate for each sample in a 10 µl final volume containing 1 µl diluted cDNA, 5 µl TaqMan Universal PCR Master Mix (Applied Biosystems), and 0.5 µl Assay-on Demand mix. The results were analyzed with a Delta-Delta CT method.

Bone resorption assay and TRAP activity

Monocytes ($0.5x10^6$) were plated in 24-well Osteo Assay Surface culture plates (Corning Inc, Corning, NY, USA) and differentiated to MDOCs as described above adding the ICOS reagents at T14 or T21. As a control, monocytes were cultured also in the absence or presence of M-CSF alone. Supernatants were then collected and the calcium level was evaluated by a calcium colorimetric assay kit (Sigma-Aldrich, St Louis, MO, USA). Moreover, erosion of the synthetic osteo-surface was visualized after staining with a modified Von Kossa method. Briefly, cells were removed from the OsteoAssay surface by incubation with 5% sodium hypochlorite for 5 min. Then, 300 µl of silver nitrate solution at 5% (w/v) was added to each well and the plate was incubated for 30 min in darkness at room temperature. Wells were then washed with distilled water and treated

with 300 µl of balanced formalin at 5% (w/v) for 5 min at room temperature. After washing with distilled water, wells were aspirated and air dried before imaging analysis (32).

Alternatively, monocytes ($0.5x10^6$) were plated in 96-well plates containing dentin disks (Pantec Srl, Torino, Italy) and differentiated to MDOCs as described above adding the ICOS reagents at T14 or T21. To analyze erosion pit formation on the dentin disk surface, the medium was aspirated from the wells and 0.25% trypsin was added for 15 minutes. Then, wells were washed twice with distilled water, incubated with 0.25 M ammonium hydroxide, and stained with 0.5% toluidine blue followed by NaOH 2N. Individual pits or pit clusters were observed using a microscope at 25 to 100x magnification and analyzed with a specific program (33).

TRAP activity was assessed using the Acid Phosphatase kit (Sigma-Aldrich) according to the manufacturer's instructions.

In vivo analysis

For RANKL-induced osteoporosis, we used 49-day old C57BL/6 female mice and groups were composed from the same littermates. Soluble RANKL (GenWay Biotech. Inc. San Diego, CA, USA; 1 mg/kg) was injected i.p. daily for 3 d (34) alone or in combination with 100 µg ICOS-msFc, or ^{F119S}ICOS-Fc. Control mice were injected with PBS or 100 µg ICOS-msFc, or ^{F119S}ICOS-Fc but not with RANKL. The mice were sacrificed 4 h after the last injection, and tibias, and femurs were collected for analysis.

For ovariectomy (OVX)-induced osteoporosis, we used 56-day old C57BL/6 female mice and groups were composed from the same littermates. Bilateral OVX was performed in mice anesthetized with a mix of Zoletil® (60mg/kg) and Xilazina® (20mg/kg) i.p, as reported (35,36). The sham-control group received the same surgical procedures except for removal of the ovaries. One day after surgery, mice were treated with seven i.p. injections (1 every 4 d for 4 wk) of either PBS or msICOS-msFc (400µg). They were sacrificed 4 d after the last injection and organs and bones were collected for analysis.

Bone samples were fixed at room temperature for 2 d in 4% phosphate buffered formaldehyde pH 6.9, and undecalcified bones were dehydrated in ethanol before performing a three-step impregnation in methylmethacrylate monomer (Merck, Darmstadt, Germany) for 3 d. Sections were cut on a Leica SP 1600 Saw Microtome and mounted on polyethylene slides.

The cut was performed on the long axis of the bone in the femur and tibia metaphysis for trabecular bone, and at the mid diaphysis for cortical bone. The sections were stained with light-green (Merck) and acid fuchsin (Sigma-Aldrich). Micrographs at 4X, 10X, 20X and 40X magnification were acquired and examined in a single blind analysis. Quantitative histomorphometric analysis was performed using micrograph obtained from 6 sections from each mouse (3 sections/leg) and analyzed with Leica imaging software (Qwin Plus V 2.6, Leica).

Measurements of cortical bone included total area of the bone (TA) and medullary area (MA) while the mineralized bone area was calculated as TA – MA and expressed as % of mineralized bone, in the total area of the bone. Measurements of trabecular bone were made in a fixed area of 0.17 mm^2 inside which the medullary area was measured and the percentage of mineralized bone calculated.

Study Approval

The mice were bred under pathogen-free conditions in the animal facility of the Department of Health Sciences and were treated in accordance with the University Ethical Committee. The study was approved by the Bioethics Committee for Animal Experimentation of the University of Piemonte Orientale (Prot. No. 3/2014). Human blood samples were obtained from healthy donors who signed their written informed consent in accordance with the Declaration of Helsinki.

Statistics

Statistical analyses were performed using ANOVA with Dunnett's test using GraphPad Instat Software (GraphPad Software, San Diego, CA, USA). Statistical significance was set at $p < 0.05$.

Results

B7h expression in OCs

Monocyte-derived OCs (MDOCs) were obtained by culturing $CD14^+$ monocytes for 21 d in differentiation medium containing M-CSF and RANKL. In order to assess the MDOCs differentiation, we evaluated the cell morphology by optical microscopy and expression of surface CD14, marking monocytes, and B7h and intracellular Cathepsin K, marking OCs, by three-color immunofluorescence and flow cytometry performed at the beginning (d0, T0) and the end (T21) of the MDOCs differentiation culture and at the intermediate (T14). The immunophenotypic analysis showed that, from T0 to T21, the cells downregulated CD14 and upregulated Cathepsin K as expected (17-21,23). The proportion of total cells expressing B7h was about 30% at T0 and slightly decreased to about 20% at T21. However, about 30% of Cathepsin K^+ cells expressed B7h and about 75% of $B7h^+$ cells expressed Cathepsin K at T21 (Fig. 1A). The morphological analysis showed that the cells acquired a spindle-like morphology at T14 (data not shown) and enlarged and fused in multinuclear cells at T21, as expected (Fig. 1B). Gating of the cytofluorimetric analyses on the cells with the highest size and granularity showed that these cells expressed B7h at T21 (Fig.1C). Moreover, expression of B7h was assessed at T21 by indirect immunofluorescence and microscopy analysis. Cells were stained after fixing and permeabilization in order to stain nuclei and detect both extra- and intracellular B7h, since both expressions have been detected in other cell types (37,38). Results showed that B7h was expressed in both mononuclear and multinuclear cells (Fig. 1C). Finally, to confirm expression of B7h, we analyzed its mRNA by Real Time PCR and the protein by western blot at T7, T14 and T21. Results confirmed that B7h expression decreased during MDOCs differentiation, but it was maintained at T21, especially at the protein level (Fig. 1D).

Effects of B7h triggering on OCs differentiation

Since B7h is expressed during the MDOCs differentiation culture, we evaluated the effect of B7h

triggering on differentiating MDOCs using ICOS-Fc. To assess the specificity of the ICOS effect, cells were also treated with either ^{F119S}ICOS-Fc, which is a mutated form of ICOS incapable of binding B7h, or ICOS-msFc, in which the human ICOS is fused with a mouse Fcγ portion to minimize interaction with the human Fcγ receptors. In preliminary experiments, we assessed the ICOS-Fc effect on monocyte proliferation by performing a MTT assay on monocytes cultured for 3 days in the presence and absence of M-CSF with and without ICOS-Fc. Results showed that ICOS-Fc had no effect on monocyte proliferation in any culture condition (Fig. S1).

Treatment of differentiating MDOCs was started at either T0 or T14 of the culture by adding the ICOS reagents to the differentiating medium. The culture was continued up to T21 to perform the $T^{0\text{-}21}$ and $T^{14\text{-}21}$ treatments (Fig. S1).

The results showed that the $T^{0\text{-}21}$ treatment with ICOS-Fc or ICOS-msFc powerfully inhibited MDOCs differentiation. At d10 (T10), cells displayed a round shape (data not shown) and, at T21, they acquired a spindle-like morphology and showed decreased the formation of multinuclear TRAP positive cells (expressed as % TRAP-positive cells) (Fig. 2A,B). Cytofluorimetric analysis showed minimal downregulation of CD14 and upregulation of Cathepsin K (Fig. 2C). By contrast, cells treated with ^{F119S}ICOS-Fc did not display any difference from untreated cells showing the typical progression toward the MDOCs morphology and phenotype.

Since a key aspect of OCs is cytoskeleton organization to form the ruffle border at the erosion area delimited by the sealing zone, we analyzed the effect of the ICOS reagents on the cell actin organization by intracellular staining of $T^{0\text{-}21}$-treated MDOCs cells with TRITC-phalloidin, which binds actin. Untreated MDOCs were giant cells with podosomes concentrated in well-organized dense actin rings, and actin was polarized with a pattern typical of the sealing zone delimiting the erosive lacuna of OCs. By contrast, in cells treated with ICOS-Fc or ICOS-msFc, cells were smaller, with podosomes arranged in noncircular clusters across the cell body, and actin displayed a perinuclear distribution in a typical F-acting ring without signs of polarization. Cells treated with ^{F119S}ICOS-Fc displayed a pattern similar to that of untreated cells (Fig. 2D).

Since OCs differentiations is marked by upregulation of DC-STAMP, OSCAR and NFATc1 expression, we assessed the effect of the T^{0-21} treatment with the ICOS reagents on the expression of these genes by Real Time PCR at T7, T14 and T21. Results showed that ICOS-Fc and ICOS-msFc decreased expression of all these mRNAs compared to untreated cells and cells treated with ^{F119S}ICOS-Fc (Fig. 3).

The T^{14-21} treatment with either ICOS-Fc or ICOS-msFc showed a substantial slowing down of MDOCs differentiation since, at T21, cells displayed decreased cell size and nuclei pyknosis, a decreased ability to adhere to the culture wells, increased number of cells with one nucleus only or ≤ 3 nuclei, and a decreased number of cells with >3 nuclei compared to untreated cells. Moreover, several cells displayed a star-like morphology that was not detected in untreated cells. Cytofluorimetric analysis showed a slight decrease of Cathepsin K upregulation and a striking decrease of CD14 downregulation, so that $CD14^{-}$Catepsin K^{+} cells were about 1% in the ICOS-Fc-treated cultures versus >50% cells in the control cultures. By contrast, cells treated with ^{F119S}ICOS-Fc were similar to untreated cells (Fig. 4). Actin staining and TRAP assay performed on these cells at T21 showed data similar to those detected in the T^{0-21} treatment (Fig. S2).

To assess reversibility of the ICOS-Fc effect, cells were treated with the different ICOS reagents at T7 washed at T14 and then incubated to T21 in the absence of the ICOS reagents (T^{7-14} treatment) (Fig. S1). The results showed that the T^{7-14} treatment induced a morphology, phenotype, actin staining and TRAP activity converging on that displayed by untreated cells (Fig. S3). By contrast, cells that, after the T14 washing, were cultured again in the presence of the ICOS reagents (T^{7-21} treatment) displayed features similar to those described above for the T^{14-21} treatment (data not shown).

Effects of B7h triggering on differentiated OCs

Treatment of already differentiated MDOCs was performed by treating cells at T21 with the ICOS reagents and analyzing them after 3 d (T24) to perform the T^{21-24} treatment (Fig. 5). The results

showed that the T^{21-24} treatment with ICOS-Fc or ICOS-msFc induced a striking decrease of the sizes of cells and nuclei and a decreased expression of Cathepsin K compared to untreated cells. By contrast, the T^{21-24} treatment with ^{F119S}ICOS-Fc did not display any effect.

To assess reversibility of the ICOS effect, T^{21-24}-treated cells were washed at T24 and incubated for 1 (T25) or 4 d (T28) in a differentiation medium in the absence of ICOS-Fc. The results showed that cells treated with ICOS-Fc or ICOS-msFc and then grown in the absence of ICOS-Fc started to enlarge and upregulated Cathepsin K at T25, and displayed a MDOC-like morphology converging on that displayed by untreated cells, at T28. By contrast, cells that had been untreated or treated with ^{F119S}ICOS-Fc maintained their morphology and phenotype at T25 and T28 (Fig. 5).

Analysis of cell viability by the Trypan blue exclusion test showed that cells were viable in all these culture conditions (data not shown).

Effect of B7h triggering on OCs function

To assess the effect of ICOS on the osteolytic activity of MODCs, we evaluated their ability to promote calcium release from crystalline calcium phosphate *in vitro*. MDOCs differentiation was induced in wells coated with a synthetic surface made of an inorganic crystalline calcium phosphate mimicking living bone material in the presence and absence of the ICOS reagents using T^{14-21} and T^{21-24} protocols. At the end of the culture, cells were washed and cultured for a further 24 h in fresh medium, with or without the ICOS reagent, and release of calcium was then assessed in the culture supernatants using a colorimetric assay. The results showed that the T^{14-21} and T^{21-24} treatments with ICOS-Fc or ICOS-msFc significantly decreased the calcium release compared with untreated MDOCs, whereas ^{F119S}ICOS-Fc did not display any effect (Fig. 6A). Moreover, we stained the surface wells with a modified Von Kossa method to visualize the erosion of the synthetic osteo-surface. Microscopic analysis showed a massive erosion in wells containing untreated MDOCs or MDOCs treated with ^{F119S}ICOS-Fc, whereas erosion was inhibited in wells containing MDOCs treated with ICOS-Fc and minimal in in wells containing monocytes cultured

in the absence or presence of M-CSF alone (Fig. 6B).

To confirm these data, we assessed the effect of ICOS on the osteolytic activity of MODCs on dentine disks. MDOCs differentiation was induced in wells containing dentin disks in the presence and absence of the ICOS reagents using T^{14-21} and T^{21-24} protocols. At the end of the culture, the disks were stained with toluidine blue and erosion pits were visualized with a microscope and quantified with a dedicated software. The results showed that the T^{14-21} and T^{21-24} treatments with ICOS-Fc significantly decreased the erosion compared with untreated MDOCs, whereas ^{F119S}ICOS-Fc did not display any effect (Fig. 6C).

To investigate the effect of B7h triggering at the signaling level, we treated MDOC at T21 in the absence and presence of either ICOS-Fc or ICOS-msFc or ^{F119S}ICOS-Fc (5 μg/ml) for 30 min, and then assessed the expression level of phospho-p38, phospho-ERK, phospho-JNK, phospho-PKC, and β-Pix, which were found to be modulated by B7h triggering in different cell types in previous works (13,15,16); expression of total p38, Erk, JNK, and β-actin was assessed as the control. The results showed that phospho-p38 was upregulated by treatment with both ICOS-Fc and ICOS-msFc but not with ^{F119S}ICOS-Fc. By contrast, no effect was detected on phospho-ERK, phospho-JNK, β-Pix, and phospho-PKC (Fig. 7).

Finally, we assessed the effect of B7h triggering *in vivo* using two mouse models of osteoporosis.

Firstly, 49-day-old female C57BL/6 mice were injected i.p. daily for 3 d with RANKL (1 mg/kg) alone or in combination with either an msICOS-huFc (formed by the mouse ICOS and the human Fc) or ^{F119S}ICOS-Fc (100 μg/mouse). The mice were sacrificed 4 h after the last injection. Histological representative images of cortical and trabecular bone stained with fucsin and light-green that evidenced fibrous and medullary tissues in red and mineralized bone in green are reported in Fig. 8A and Fig. S4. Morphometric measurements of mineralized bone tissue in the cortical and trabecular bone showed a marked bone loss in the RANKL-injected mice compared to control mice (Fig. 8B), as expected (34). This bone loss was significantly inhibited by co-treatment of mice with RANKL plus msICOS-huFc but not with RANKL plus ^{F119S}ICOS-Fc. By contrast,

383 treatment of mice with msICOS-huFc or ^{F119S}ICOS-Fc alone in the absence of RANKL had no
384 effect on the proportion of bone area.
385 Secondly, 56-day-old female C57BL/6 mice received surgery with OVX or without OVX (sham
386 controls) and, after 24 hr, were injected i.p. every 4 d for 4 wk with either PBS or a total mouse
387 ICOS-Fc (formed by the mouse ICOS and the mouse Fc). The mice were sacrificed 4 d after the last
388 injection. Morphometric measurements of mineralized bone tissue showed a marked bone loss in
389 the PBS-injected mice and the bone loss was significantly inhibited by the treatment with ICOS-Fc.
390 In the sham mice, no bone loss was detected and treatment with ICOS-Fc did not show any effect
391 (Fig. 9A-B). To evaluate whether the ICOS-Fc effect was ascribable to decreased OCs activity, we
392 evaluated expression of DC-STAMP and NFATc1 in the mRNA extracted from these bones by
393 Real Time PCR. Results, showed that the treatment with ICOS-Fc significantly decreased the levels
394 of DC-STAMP and NFATc1 compared to the controls. In the sham mice, levels of DC-STAMP and
395 NFATc were significantly lower than in control OVX mice and were not modulated by treatment
396 with ICOS-F (Fig. 9C).
397

Discussion

Bone remodeling is a complex process managed by OBs and OCs, and the immune system is involved in regulating the function of these cells through the activity of cytokines and surface receptors. This paper has described a novel pathway involved in the lymphocyte/bone cell interactions by showing that the binding of ICOS, expressed by activated T cells, to its ligand B7h, expressed by OCs, inhibits OCs maturation and function. These effects were detected using ICOS-Fc and they were specific, since they were not displayed by ^{F119S}ICOS-Fc incapable of binding B7h.

The effect on OCs differentiation was detected by treating cells with ICOS-Fc during the *in vitro* differentiation of monocytes to OCs. ICOS-Fc almost completely blocked the differentiation when treatment was started at the beginning of the three-weeks differentiating culture, but it inhibited the differentiation also when the treatment was started in the last week, as shown by the decreased cell multinuclearity and the arrest of acquirement of the OCs features induced by treatment with ICOS-Fc. This effect was not due to cell toxicity since cell survival was normal even when cultures were prolonged for a fourth week (data not shown). Moreover, the effect was reversible since interruption of the treatment in the last week of culture allowed cells to restart the OCs differentiation path. The arrest of differentiation was accompanied by an altered organization of the actin cytoskeleton which, in ICOS-Fc treated cells, displayed a perinuclear distribution in a F-acting ring without the signs of polarization typical of the sealing zone delimiting the erosive lacuna detected on OCs. In line with these data, cells treated with ICOS-Fc displayed decreased expression of TRAP, OSCAR, DC-STAMP, and NFATc1, and decreased osteolytic activity *in vitro*.

A second key point was the effect of ICOS-Fc on already differentiated OCs, in which treatment with ICOS-Fc induced a striking decrease in the sizes of cells and nuclei and osteolytic activity *in vitro* without substantial effects on cell viability. Again, the effect was reversible since cells reenlarged and reassumed the OCs phenotype upon interruption of the treatment.

In differentiated OCs, B7h-mediated signaling seems to involve phosphorylation of the p38 MAPK, which marks a difference from DC in which B7h signaling involves JNK and PKC (14). Another difference was that OCs did not show the down modulation of β-Pix that had instead been detected in DC and tumor cell lines (13,16). These signaling differences parallel functional differences displayed by these cell types since B7h triggering supports DC function by costimulating cytokine secretion in activated DC whereas it inhibits differentiation of OCs (12-14). The effect of B7h on p38 is in line with the key role ascribed to p38 in osteoclastogenesis since, on the one hand, RANKL-induced osteoclastogenesis involves activation of the ERK, JNK, and p38 pathway, and on the other hand, OPG performs part of its anti-osteoclastogenic activity by inducing p38 phosphorylation and altering the balance among the ERK, JNK and p38 pathways needed for osteoclastogenesis (39-40).

These effects on OCs differentiation and function *in vitro* were supported by the *in vivo* results showing that treatment with ICOS-Fc strikingly inhibits the systemic bone resorption induced in mice by high doses of soluble RANKL or ovariectomy (34).

The observation that the ICOS/B7h interaction can modulate OCs function is in line with the notion that several components of the immune system, including T cells, are able to modulate bone formation. Moreover, bone loss is a common feature of several chronic inflammatory and autoimmune diseases since the risk of osteoporosis is increased in patients with RA, inflammatory bowel disease and systemic lupus erythematosus, and aggressive localized bone destruction can be a feature of certain autoimmune diseases, cancers, and infections (42,43). In RA patients, the localized bone losses may involve inflammatory cytokines such as IL-1, IL-6, and TNFα, which are abundant in synovial fluid and synovium and can induce RANKL on synovial fibroblasts and stromal cells. Moreover, RANKL expressed by T and B cells in the synovial tissue and fluid can be involved in OCs activation (44). Intriguingly, even the osteoporosis due to menopausal estrogen deficiency may involve increased production of inflammatory cytokines such as TNFα and IL-17 and increased RANKL expression on B and T cells (45).

In the immune control of bone formation, a key role has been ascribed to T helper (Th) cells. Th1 and Th2 cells secrete IFNγ and IL-4, respectively, which are anti-osteoclastogenic cytokines (43). By contrast, Th17 cells express high levels of RANKL and secrete IL-17, inducing expression of RANKL on mesenchymal cells and recruitment of inflammatory cells (43). Moreover, Th17 cells secrete also IL-22, which may induce OB differentiation, enhancing bone formation at sites of inflammation. The cells may also act by use of surface receptors, since their CD40L can stimulate CD40 expressed on stromal cells inducing them to upregulate RANKL and downmodulate OPG expression and, therefore, support OCs function (46). Moreover, regulatory T (Treg) cells can inhibit osteclastogenesis by release of TGF-β and surface expression of CTLA4 whose interaction with B7.1 and B7.2 on monocyte prevents their differentiation to OCs (47). The Treg role in inhibiting OCs differentiation is in line with the anti-osteoclastogenic activity of ICOS because not only do subsets of Treg cells express high levels of ICOS, but also ICOS triggering is involved in Treg differentiation (48). A cooperative role of ICOS and CTLA4 in inhibition of OCs function would be intriguing, since both molecules belong to the CD28 family, bind surface receptors belonging to the B7 family, and are involved in Treg function. The anti-osteoclastogenic activity displayed by ICOS and CTLA4 may counteract the pro-osteoclastogenic activity displayed by T cells by expression of RANKL, CD40L, and IL-17, and the overall effect may depend on the balance between these different signals (49). These data open a novel field in the pharmacological use of agonists and antagonists of the ICOS/B7h system which to date have been envisaged as immune modulators mainly in the fields of autoimmune diseases and anti-tumor immune response.

A**cknowledgments**

Contributions: U.D., G.I., and C.D. designed research; C.L.G., E.B., N.C., and Y.S. performed research; E.T., and D.S. contributed reagents/tools; P.D.A., A.C., R.B., and M.B. analyzed data; U.D., J.Y., and, J.M.R. wrote the paper.

Disclosure

A patent application (Italy: n.102015000018209; International: n. PCT/IB2016/052903) has been submitted for use of ligands of B7h receptor in the treatment of osteopenia and osteoporosis.

References

1. Swallow, M. M., J. J. Wallin, and W. C. Sha. 1999. B7h, a novel costimulatory homolog of B7.1 and B7.2, is induced by TNFalpha. *Immunity*. 11: 423-432.

2. Redoglia, V., U. Dianzani, J. M. Rojo, P. Portoles, M. Bragardo, H. Wolff, D. Buonfiglio, S. Bonissoni, and C. A. Janeway Jr. 1996. Characterization of H4: a murine T lymphocyte activation molecule functionally associated with the CD3/TCR. *Eur. J. Immunol.* 26: 2781-2789.

3. Hutloff, A., A. M. Dittrich, K. C. Beier, B. Eljaschewitsch, R. Kraft, I. Anagnostopoulos, and R. A. Kroczek. 1999. ICOS is an inducible T cell co-stimulator structurally and functionally related to CD28. *Nature.* 397: 263-266.

4. Buonfiglio, D., M. Bragardo, V. Redoglia, R. Vaschetto, F. Bottarel, S. Bonissoni, T. Bensi, C. Mezzatesta, C. A. Janeway Jr, and U. Dianzani. 2000. The T cell activation molecule H4 and the CD28-like molecule ICOS are identical. *Eur. J. Immunol.* 30: 3463-3467.

5. Greenwald, R. J., G. J. Freeman, and A. H. Sharpe. 2005. The B7 family revisited. *Nat. Rev. Immunol.* 23: 515-548.

6. Yagi, J., Y. Arimura, U. Dianzani, T. Uede, T. Okamoto, and T. Uchiyama. 2003. Regulatory roles of IL-2 and IL-4 in H4/inducible costimulator expression on activated CD4+ T cells during Th cell development. *J. Immunol.* 171: 783-794.

7. Park, H., Z. Li, X. O. Yang, S. H. Chang, R. Nurieva, Y. H. Wang, Y. Wang, L. Hood, Z. Zhu, Q. Tian, and C. Dong. 2005. A distinct lineage of CD4 T cells regulates tissue inflammation by producing interleukin 17. *Nat. Immunol*. 6: 1133-1141.

8. Mesturini, R., S. Nicola, A. Chiocchetti, I. S. Bernardone, L. Castelli, T. Bensi, M. Ferretti, C. Comi, C. Dong, J. M. Rojo, J. Yagi, and U. Dianzani. 2006. ICOS cooperates with CD28, IL-2, and IFN-gamma and modulates activation of human naïve CD4+ T cells. *Eur. J. Immunol*. 36: 2601-2612.

9. Mesturini, R., C. L. Gigliotti, E. Orilieri, G. Cappellano, M. F. Soluri, E. Boggio, A. Woldetsadik, C. Dianzani, D. Sblattero, A. Chiocchetti, J. Yagi, J. M. Rojo, and U. Dianzani.

2013. Differential induction of IL-17, IL-10, and IL-9 in human T helper cells by B7h and B7.1. *Cytokine*. 64: 322-330.

10. Mak, T. W., A. Shahinian, S. K. Yoshinaga, A. Wakeham, L. M. Boucher, M. Pintilie, G. Duncan, B.U. Gajewska, M. Gronski, U. Eriksson, B. Odermatt, A. Ho, D. Bouchard, J. S. Whorisky, M. Jordana, P. S. Ohashi, T. Pawson, F. Bladt, and A. Tafuri. 2003. Costimulation through the inducible costimulator ligand is essential for both T helper and B cell functions in T cell-dependent B cell responses. *Nat. Immunol.* 4: 765-772.

11. Tafuri, A., A. Shahinian, F. Bladt, S. K. Yoshinaga, M. Jordana, A. Wakeham, L. M. Boucher, D. Bouchard, V. S. Chan, G. Duncan, B. Odermatt, A. Ho, A. Itie, T. Horan, J. S. Whoriskey T. Pawson, J. M. Penninger, P. S. Ohashi, and T. W. Mak. 2001. ICOS is essential for effective T-helper-cell responses. *Nature.* 409: 105-109.

12. Tang, G., Q. Qin, P. Zhang, G. Wang, M. Liu, Q. Ding, Y. Qin, and Q. Shen. 2009. Reverse signaling using an inducible costimulator to enhance immunogenic function of dendritic cells. *Cell Mol. Life Sci*. 66: 3067-3080.

13. Occhipinti, S., C. Dianzani, A. Chiocchetti, E. Boggio, N. Clemente, C. L. Gigliotti, M. F. Soluri, R. Minelli, R. Fantozzi, J. Yagi, J. M. Rojo, D. Sblattero, M. Giovarelli, and U. Dianzani. 2013. Triggering of B7h by the inducible costimulator modulates maturation and migration of monocyte-derived dendritic cells. *J. Immunol.* 190: 1125-1134.

14. Hedl, M., A. Lahiri, K. Ning, J. H. Cho, and C. Abraham. 2014. Pattern recognition receptor signaling in human dendritic cells is enhanced by ICOS ligand and modulated by the Crohn's disease ICOSLG risk allele. *Immunity.* 40: 734-746.

15. Dianzani, C., R. Minelli, R. Mesturini, A. Chiocchetti, G. Barrera, S. Boscolo, C. Sarasso, C. L. Gigliotti, D. Sblattero, J. Yagi, J. M. Rojo, R. Fantozzi, and U. Dianzani. 2010. B7h triggering inhibits umbilical vascular endothelial cell adhesiveness to tumor cell lines and polymorphonuclear cells. *J. Immunol*. 185: 3970-3979.

16. Dianzani, C., R. Minelli, C. L. Gigliotti, S. Occhipinti, M. Giovarelli, L. Conti, E. Boggio, Y. Shivakumar, G. Baldanzi, V. Malacarne, E. Orilieri, G. Cappellano, R. Fantozzi, D. Sblattero, J. Yagi, J. M. Rojo, A. Chiocchetti, and U. Dianzani. 2014. B7h triggering inhibits the migration of tumor cell lines. *J. Immunol.* 192: 4921-4931.

17. Teitelbaum, S. L. 2011. The osteoclast and its unique cytoskeleton. *Ann. N Y Acad. Sci.* 1240: 14-17.

18. Teti, A. 2011. Bone development: overview of bone cells and signaling. *Curr. Osteoporos. Rep.* 9: 264-273.

19. Väänänen, H. K., H. Zhao, M. Mulari, and J. M. Halleen. 2000. The cell biology of osteoclast function. *J. Cell Sci.* 113: 377-381.

20. Ikeda, K., and S. Takeshita. 2014. Factors and mechanisms involved in the coupling from bone resorption to formation: how osteoclasts talk to osteoblasts. *J. Bone Metab.* 21: 163-167.

21. Charles, J. F., and A. O. Aliprantis. 2014. Osteoclasts: more than 'bone eaters'. *Trends Mol. Med.* 20: 449-459.

22. Burgess, T. L., Y. Qian, S. Kaufman, B. D. Ring, G. Van, C. Capparelli, M. Kelley, H. Hsu, W. J. Boyle, C. R. Dunstan, S. Hu, and D. L. Lacey. The ligand for osteoprotegerin (OPGL) directly activates mature osteoclasts. *J. Cell Biol.* 145: 527-538.

23. Boyle, W. J., W. S. Simonet, and D. L. Lacey. 2003. Osteoclast differentiation and activation. *Nature.* 423: 337-342.

24. Ferrari, S. 2014. Future directions for new medical entities in osteoporosis. *Best. Pract. Res. Clin. Endocrinol. Metab.* 28: 859-870.

25. Walsh, M. C., and Y. Choi. 2014. Biology of the RANKL-RANK-OPG System in Immunity, Bone, and Beyond. *Front. Immunol.* 5:511.

26. Zhang, J., J. Dai, Y. Qi, D. L. Lin, P. Smith, C. Strayhorn, A. Mizokami, Z. Fu, J. Westman, and E. T. Keller. 2001. Osteoprotegerin inhibits prostate cancer-induced osteoclastogenesis and prevents prostate tumor growth in the bone. *J. Clin. Invest.* 107: 1235-1244.

27. Nakashima, T., and H. Takayanagi. 2009. Osteoimmunology: crosstalk between the immune and bone systems. *J. Clin. Immunol.* 29: 555-567.

28. Vis, M., M. Güler-Yüksel, and W. F. Lems. 2013. Can bone loss in rheumatoid arthritis be prevented? *Osteoporos. Int.* 24: 2541–2553.

29. Okamoto, K., and H. Takayanagi. 2011. Osteoclasts in arthritis and Th17 cell development. *Int. Immunopharmacol.* 11: 543-548.

30. Tucci, M., S. Stucci, A. Savonarola, S. Ciavarella, P. Cafforio, F. Dammacco, and F. Silvestris F. 2013. Immature dendritic cells in multiple myeloma are prone to osteoclast-like differentiation through interleukin-17A stimulation. *Br. J. Haematol.* 161: 821-831.

31. Marino, S., J. G. Logan, D. Mellis, and M. Capulli. 2014. Generation and culture ofosteoclasts. *Bonekey Rep*. 570: 1-9.

32. Wang, Y., X Xu, H.B. Wang, D. Wu, X.O. Li, Q. Peng, N. Liu, W.C. 2015. Sun. 17-Hydroxy-jolkinolide A inhibits osteoclast differentiation through suppressing the activation of NF-κB and MAPKs. *Int. Immunopharmacol*. 29: 513-20.

33. Brianza, S., C. Bignardi, A. Grimaldi, G.P. Pescarmona, and G.C. Isaia. Dedicated image analysis software tool for the evaluation of the resorption activity of cultured osteoclasts. *J. Imaging Sci. Technol.* 52: 030508–030508-9.

34. Tomimori, Y., K. Mori, M. Koide, Y. Nakamichi, T. Ninomiya, N. Udagawa, and H. Yasuda. 2009. Evaluation of pharmaceuticals with a novel 50-hour animal model of bone loss. *J. Bone Miner. Res.* 24: 1194-1205.

35. Moran, A., G.L. Warren, and D.A. Lowe. 2006. Removal of ovarian hormones from mature mice detrimentally affects muscle contractile function and myosin structural distribution. *J Appl. Physiol. (1985)*. 100: 548–559.

580 36. Greising, S.M., K.A. Baltgalvis, A.M. Kosir, A.L. Moran, G.L. Warren, and D.A. Lowe. 2011.
581 Estradiol's beneficial effect on murine muscle function is independent of muscle activity. *J*
582 *Appl. Physiol.. (1985)*. 110: 109-115.
583 37. Wiendl, H., M. Mitsdoerffer, D. Schneider, A. Melms, H. Lochmuller, R. Hohlfeld, and M.
584 Weller. 2003. Muscle fibres and cultured muscle cells express the B7.1/2-related inducible co-
585 stimulatory molecule, ICOSL: implications for the pathogenesis of inflammatory myopathies.
586 *Brain.* 126: 1026-1035.
587 38. Wahl, P., R. Schoop, G. Bilic, J. Neuweiler, M. Le Hir, S. K. Yoshinaga, and R. P. Wüthrich.
588 2002. Renal tubular epithelial expression of the costimulatory molecule B7RP-1 (inducible
589 costimulator ligand). *J. Am. Soc. Nephrol.* 13: 1517-1526.
590 39. Theoleyre, S., Y. Wittrant, S. Couillaud, P. Vusio, M. Berreur, C. Dunstan, F. Blanchard, F.
591 Rédini, and D. Heymann. 2004. Cellular activity and signaling induced by osteoprotegerin in
592 osteoclasts: involvement of receptor activator of nuclear factor kappaB ligand and MAPK.
593 *Biochim. Biophys. Acta.* 1644: 1-7.
594 40. Seshasayee, D., H. Wang, W. P. Lee, P. Gribling, J. Ross, N. Van Bruggen, R. Carano, and I. S.
595 Grewal. 2004. A novel in vivo role for osteoprotegerin ligand in activation of monocyte
596 effector function and inflammatory response. *J. Biol. Chem.* 279: 30202-30209.
597 41. Takayanagi, H. 2007. Osteoimmunology: shared mechanisms and crosstalk between the
598 immune and bone systems. *Nat. Rev. Immunol.* 7: 292-304.
599 42. Danks, L., and H. Takayanagi. 2013. Immunology and bone. *J. Biochem.* 154: 29-39.
600 43. Greenblatt, M. B., and J. H. Shim. 2013. Osteoimmunology: a brief introduction. *Immune Netw.*
601 13: 111-115.
602 44. Komatsu, N., and H. Takayanagi. 2012. Autoimmune arthritis: the interface between the
603 immune system and joints. *Adv. Immunol.* 115: 45-71.
604 45. Faienza, M. F., A. Ventura, F. Marzano, and L. Cavallo. 2013. Postmenopausal osteoporosis:
605 the role of immune system cells. *Clin. Dev. Immunol.* 575936.

606 46. Lopez-Granados, E., S. T. Temmerman, L. Wu, J. C. Reynolds, D. Follmann, S. Liu, D. L.
607 Nelson, F. Rauch, and A. Jain. 2007. Osteopenia in X-linked hyper-IgM syndrome reveals a
608 regulatory role for CD40 ligand in osteoclastogenesis. *Proc. Natl. Acad. Sci. U S A.* 104: 5056-
609 5061.
610 47. Axmann, R., S. Herman, M. Zaiss, S. Franz, K. Polzer, J. Zwerina, M. Herrmann, J. Smolen,
611 and G. Schett. 2008. CTLA-4 directly inhibits osteoclast formation. *Ann. Rheum. Dis.* 67: 1603-
612 1609.
613 48. Zhang, H., H. Kong, X. Zeng, L. Guo, X. Sun, and S. He. 2014. Subsets of regulatory T cells
614 and their roles in allergy. *J. Transl. Med.* 12: 125.
615 49. Nurieva, R. I., X. Liu, and C. Dong. 2009. Yin-Yang of costimulation: crucial controls of
616 immune tolerance and function. *Immunol. Rev.* 229: 88-100.
617
618

Figure Legends

FIGURE 1

B7h expression on MDOCs. Monocytes were cultured in the presence of M-CSF and RANKL for 21 d. (**A**) Flow cytometry of CD14, B7h, and Catepsin-K expression in cells at T0, and T21. Numbers in each panel indicate the % of positive cells vs the corresponding negative control (representative of 5 experiments). The FSC and SSC parameters indicate cell size and granularity respectively. **(B)** Phase-contrast microscopy of cells at d 0 (T0) and d 21 (T21) of culture. (**C**) *(Upper panel)* Cytofluorimetric analysis of B7h (white) and control (black) staining of the large/granular cells gated from the FSC/SSC plots shown in panel A; cells from gate R1 are shown in the left, those from gate R2 in the right. *(Lower panel)*. Microphotograph of fixed and permeabilized cells stained with a polyclonal anti-B7h antibodies (left) or pre-immune rabbit Ig (right) plus a Texas Red-conjugated secondary antibody (red) and DAPI (blue, marking the nuclei) at T21 (representative of 3 experiments). Scale bar: 50 μm. (**D**) B7h expression level evaluated as mRNA by real time PCR (*left panel*) and protein by western blot (*right panel*) at T7, T14, and T21. A Data are expressed as the mean±SEM of the percentage of the expression from 3 independent experiments. (*: $p<0.05$). A representative western blot is also shown.

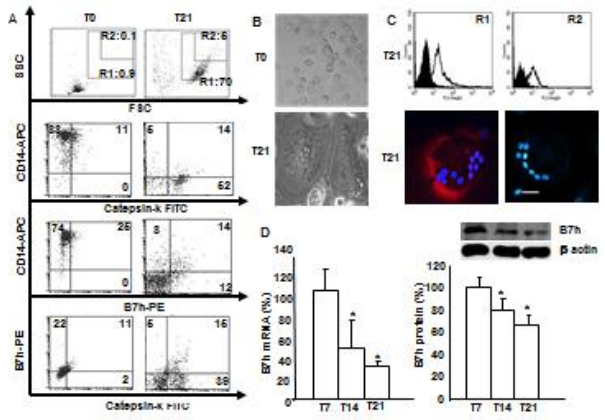

Figure 1

FIGURE 2

Effect of ICOS-Fc on MDOCs differentiation using the T^{0-21} treatments. Monocytes were induced to differentiate to MDOCs in the presence and absence of the ICOS reagents added from d0 (T^{0-21} treatment). (**A**) Microphotographs of TRAP staining at T21 (representative of 3 experiments). (**B**) The bar graphs show the % of the multinuclear $TRAP^+$ cells at T21. Data are expressed as the mean±SEM of the percentage of inhibition versus the control (set at 100%) obtained in 3 independent experiments by counting 10 fields/sample (*: $p<0.05$ versus the control). **(C)** Flow cytometry of CD14 and Catepsin-K expression at T21. Numbers in each panel indicate the % of positive cells vs the internal negative control (representative of 5 experiments). (**D**) Fluorescent microscopy of cells stained with TRITC-phalloidin (red, marking actin) and DAPI (blue, marking the nuclei) at T21 (representative of 3 experiments). Big arrows indicate sealing zone of polarized mature OCs; small arrows indicate podosomes arranged in non circular clusters across the cell body in non polarized immature OCs.

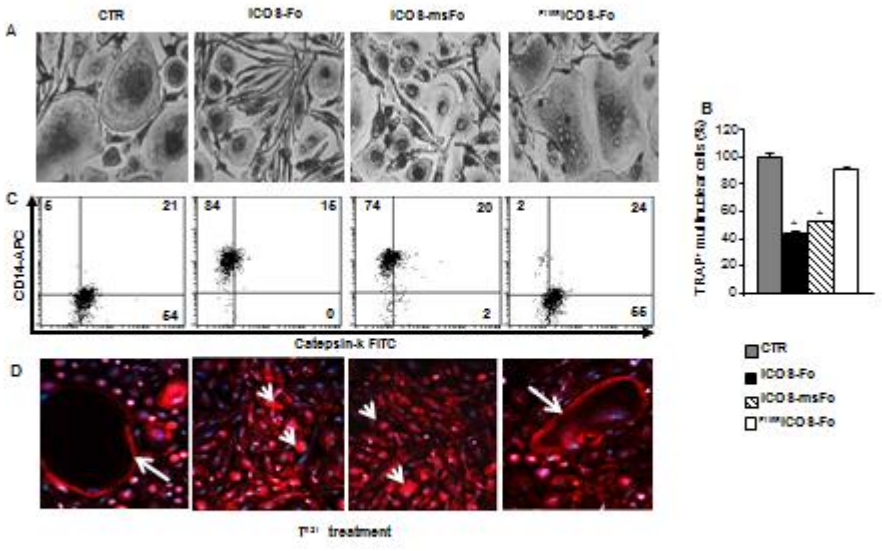

Figure 2

FIGURE 3

Effect of ICOS-Fc on MDOCs expression of OSCAR, NFATc1, and DC-STAMP using the T^{0-21} treatments. The bar graphs show the real Time PCR data of expression of OSCAR (*upper panel*), NFATc1 (*middle panel*), and DC-STAMP (*lower panel*) at T7, T14, and T21. Data are expressed as the mean±SEM from 3 independent experiments. The data are normalized for the expression in the control cells (control expression set at 100%). (*: $p<0.05$, **: $p<0.01$ versus the control).

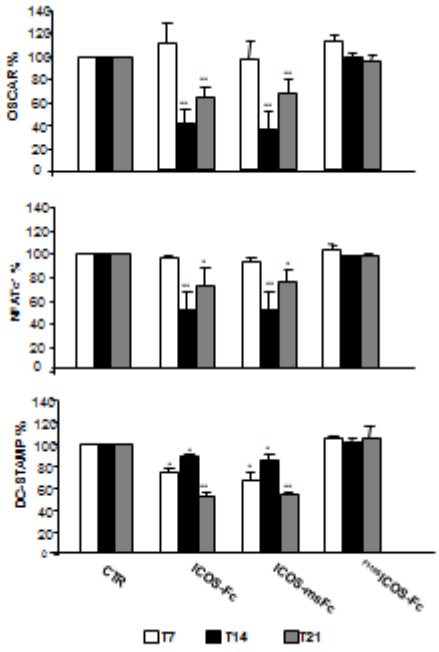

Figure 3

FIGURE 4

Effect of ICOS-Fc on the late MDOCs differentiation using the $T^{14\text{-}21}$ treatment. Monocytes were induced to differentiate to MDOCs in the presence and absence of the ICOS reagents added from T14. (**A**) Phase-contrast microscopy of cells at T21. (**B**) Flow cytometry of CD14 and Catepsin-K expression at T21. Numbers in each panel indicate the % of positive cells vs the internal negative control (representative form 3 experiments). (**C**) The bar graphs show the number of nuclei counted in each field at T21 (mean from 5 fields); data are expressed as the mean±SEM from 3 independent experiments (*: $p<0.05$ versus the control).

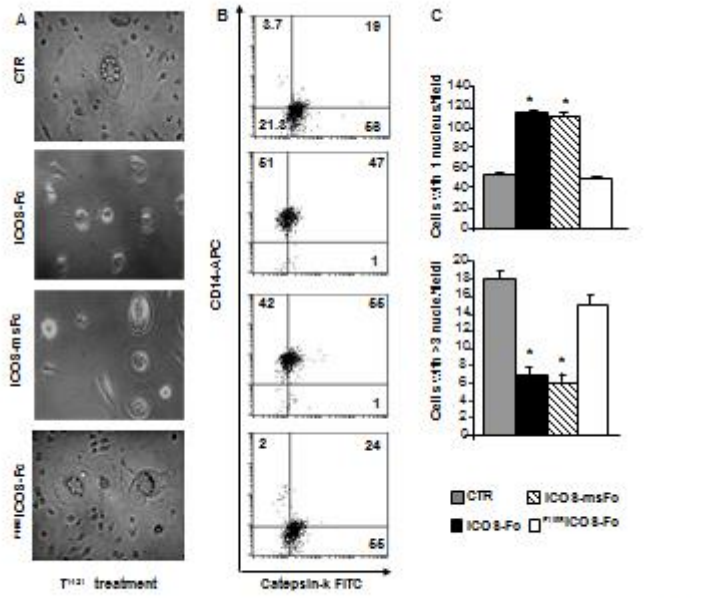

Figure 4

FIGURE 5

Effect of ICOS-Fc on differentiated MDOCs. After the 21 d differentiating culture, MDOCs were cultured in the presence and absence of the ICOS reagents for a further 3 d (T^{21-24} treatment), washed and then cultured for a further 4 d (T25-T28). (**A**) Phase-contrast microscopy and (**B**) flow cytometry of CD14 and Catepsin-K expression at T24, T25, and T28. Panels are representative of 3 experiments.

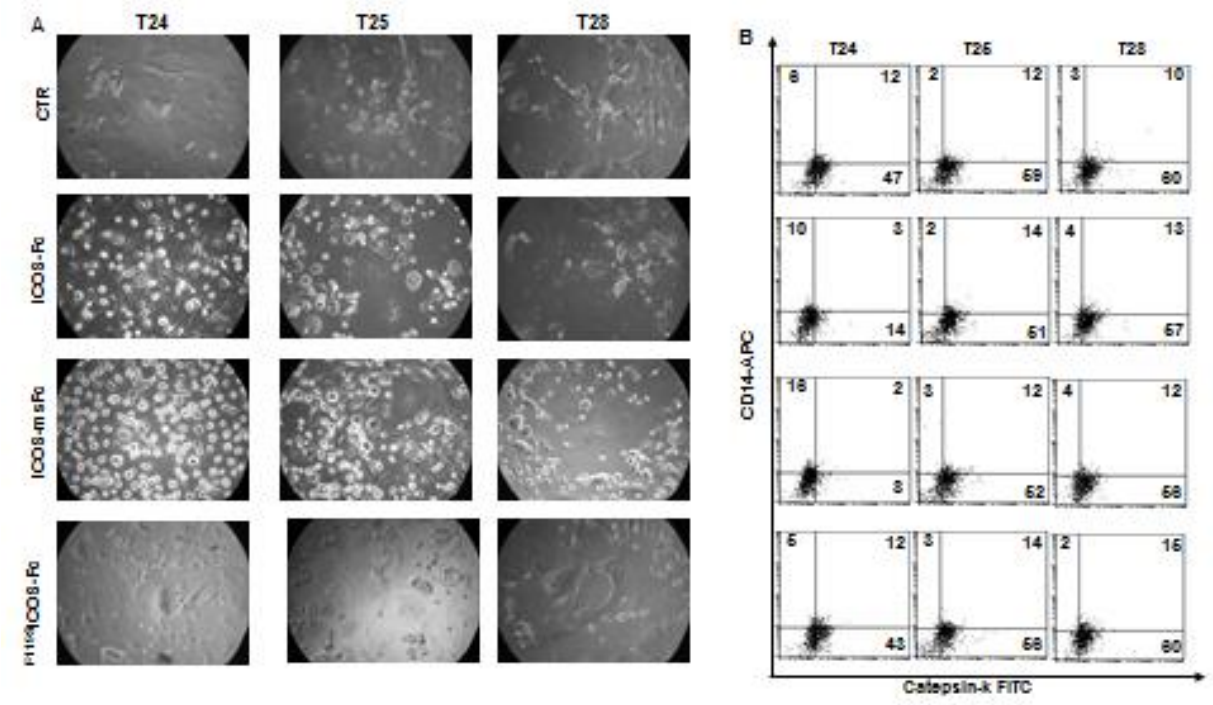

Figure 5

FIGURE 6

Effect of B7h triggering on osteolytic activity in MDOCs. MDOCs differentiating from monocytes were treated with or without the ICOS reagents added from T14 (T^{14-21} treatment) or T21 (T^{21-24} treatment). (**A**) MDOCs differentiation was induced on OsteoSurface plates; at the end of the culture, wells were washed and calcium release was evaluated in the following 24 h. Data represent the mean±SEM of the percentage of inhibition versus the control from 4 independent experiments

684 performed in duplicate. (*: p<0.05 vs the control). **B**) The graphs show the measure of the resorbed
685 area from the calcium matrix of OsteoSurface plates in the T^{14-21} treatment. The control and M-CSF
686 bars show the data obtained with monocytes cultured in the absence and presence of M-CSF alone,
687 respectively. Representative images of the wells are also shown; erosion areas appear lightly
688 coloured. Data represent the mean±SEM of the resorbed area from 4 independent experiments
689 performed in duplicate; percentages indicate the proportion of resorbed area (*: p<0.05 vs the
690 control). (**C**) MDOCs differentiation was induced on dentin disks. The bar graphs show the
691 proportion of erosion in the T^{14-21} and T^{21-24} treatments. Representative images of the disks are
692 shown for the T^{21-24} treatment. Data represent the mean±SEM from 3 experiments (*: p<0.05 vs the
693 control)..
694

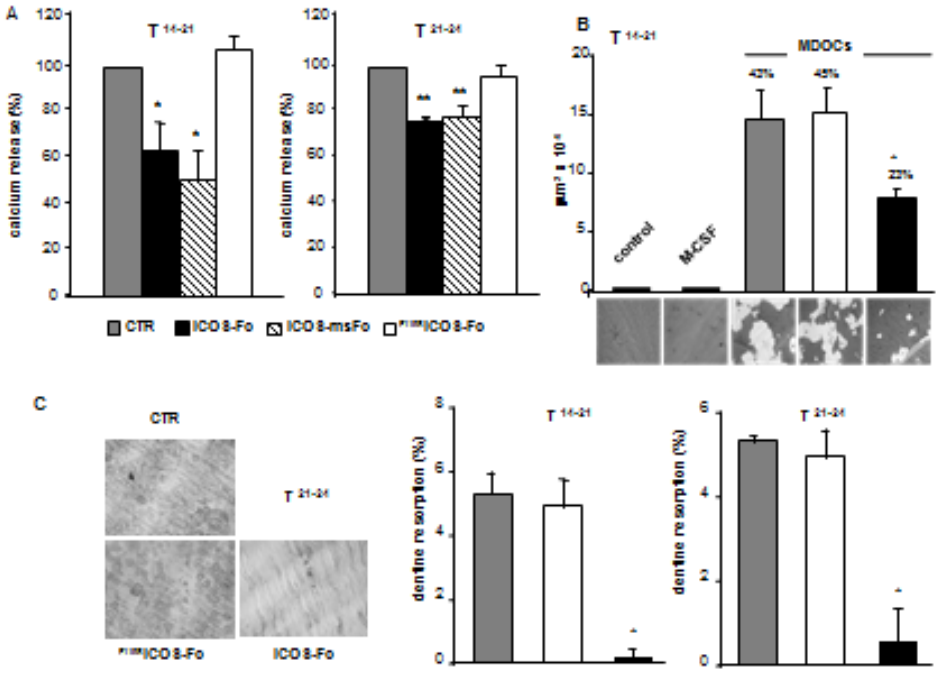

Figure 6

695
696

FIGURE 7

Effect of B7h triggering on signalling in MDOCs. Differentiated MDOCs were treated or not with the ICOS reagents (5 µg/ml) for 30 min at T21. Then, expression of (**A**) phospho-p38, (**B**) phospho-Erk1,2, (**C**) phospho-JNK, (**D**) β-Pix, and (**E**) phospho-PKC were assessed by western blot. The same blots were also probed with anti p38, Erk1,2, JNK or anti β-actin antibody as controls. The bar graphs show the densitometric analyses of the gels referred to the relative internal control; data are expressed as mean±SEM of the percentage of increase versus the control from 3 independent experiments (* P<0.05 versus the control).

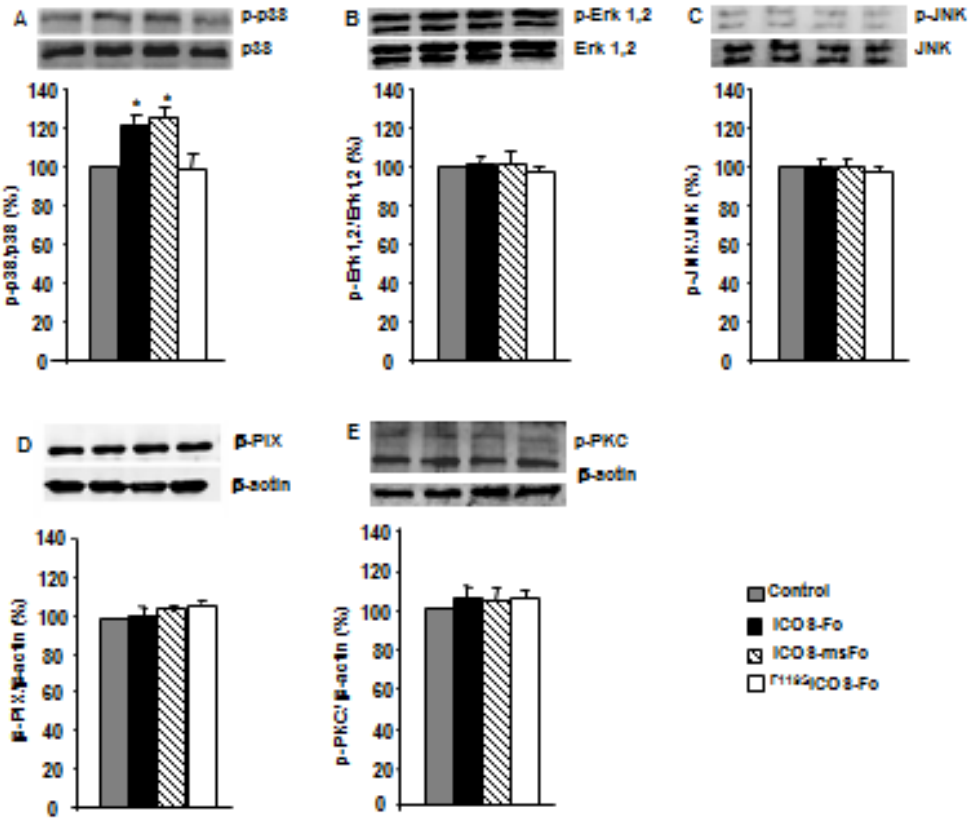

Figure 7

FIGURE 8

Effects of treatment with ICOS-Fc in a RANKL-induced mouse model of osteoporosis. Mice were injected with RANKL together with either mouse ICOS-Fc (msICOS-huFc) (n=6), or human ^{F119S}ICOS-Fc (n=6) or PBS (control group, n=6). Mice were sacrificed 4h after the last injection. Fucsin/Light green stained undecalcified sections were observed at 10X magnification in the

proximal tibia metaphysis for the trabecular bone and at 40X magnification in the tibia and fibula mid-diaphysis for the cortical bone. (**A**) Representative images of trabecular (*upper panels*) and cortical (*lower panels*) bone from mice treated with ICOS-Fc+RANKL or RANKL alone. The ICOS-Fc+RANKLpicture was similar to that detected in mice treated with either PBS or ICOS-Fc alone or ^{F119S}ICOS-Fc alone; the RANKL alone picture was similar to that detected in mice treated with ^{F119S}ICOS-Fc+RANKL (see Fig S4). (**B**) Bar graphs show the proportion of calcified bone in the trabecular (*upper panel*) and cortical (*lower panels*) region; data are mean±SEM of data obtained from 6 sections from each mouse (3 sections/leg) (**: $p<0.01$ versus control mice receiving no treatments; °°: $p<0.01$ versus mice treated with RANKL).

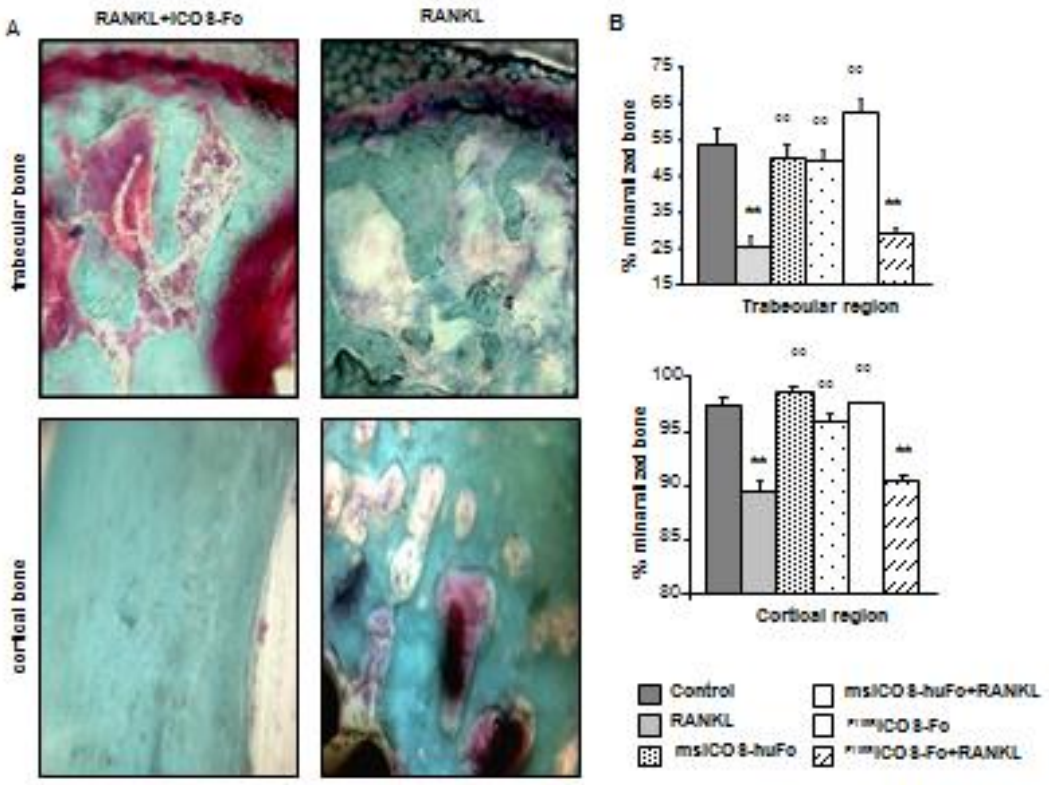

Figure 8

FIGURE 9

Effects of treatment with ICOS-Fc in a mouse osteoporosis induced by OVX. Mice received surgery and, 24 h later, were treated with ICOS-Fc (msICOS-msFc) (OVX n=6; sham n=6) or PBS

(OVX n=6; sham n=6) for 4 wk. (**A**) Representative images of cortical (*left panels*) and trabecular (*right panels*) bone from OVX mice treated with PBS (control) or ICOS-Fc, and sham mice treated with PBS; images from sham mice treated with ICOS-Fc were similar to that shown for the corresponding control treatment. Sections were observed at 4X magnification for the trabecular bone and at 25X magnification for the cortical bone. (**B**) Proportion of calcified bone in the cortical (*left panels*) and trabecular (*right panels*) region evaluated in 6 sections from each mouse (3 sections/leg). (**C**). Expression of DC-STAMP and NFATc1 evaluated by real time PCR in the cortical (*left panels*) and trabecular (*right panels*) bone (data are normalized for the expression in the OVX control group, set at 100%). Data are expressed as the mean±SEM. (***: $p<0.001$, **: $p<0.01$, *: $p<0.05$ versus the OVX control).

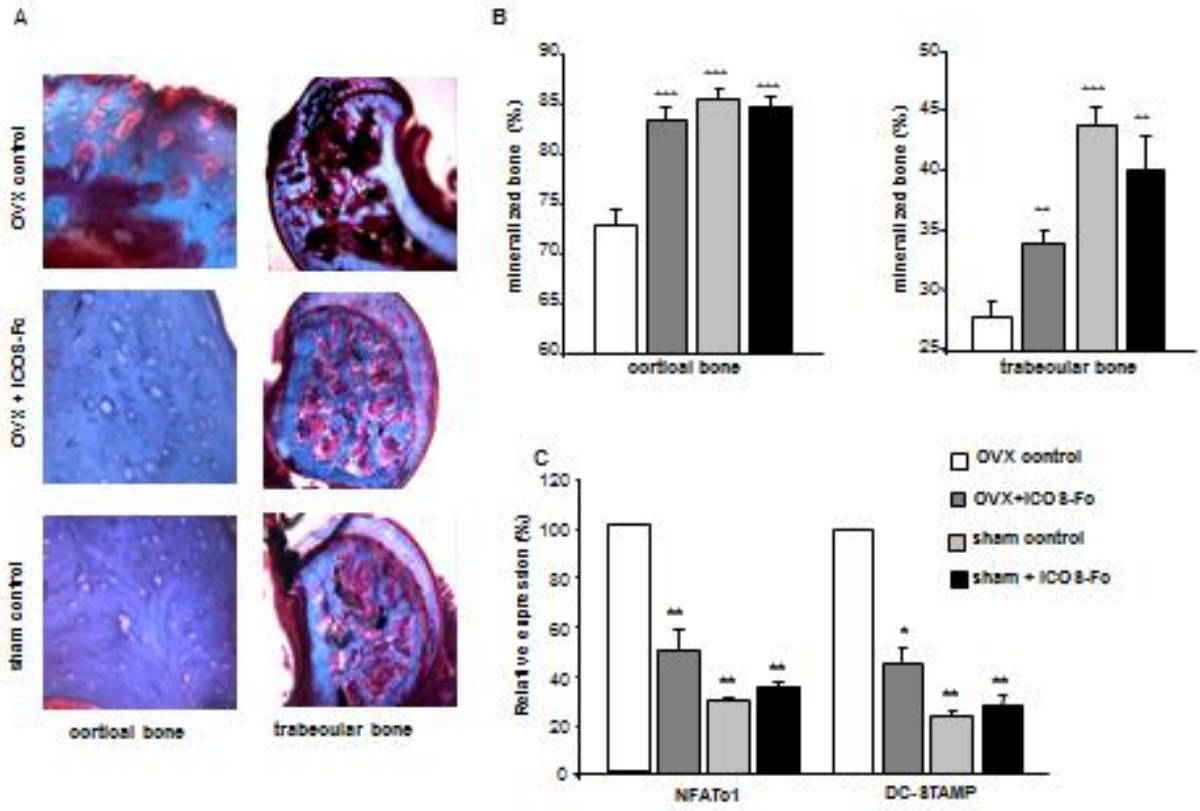

Figure 9